

Dynamic structure factor of one-dimensional Fermi superfluid with spin-orbit couplingZheng Gao ¹, Lianyi He ², Huaisong Zhao ^{1,*}, Shi-Guo Peng ^{3,†} and Peng Zou ^{1,‡}¹*College of Physics, Qingdao University, Qingdao 266071, China*²*Department of Physics, Tsinghua University, Beijing 100084, China*³*State Key Laboratory of Magnetic Resonance and Atomic and Molecular Physics,**Innovation Academy for Precision Measurement Science and Technology, Chinese Academy of Sciences, Wuhan 430071, China*

(Received 19 October 2022; accepted 4 January 2023; published 12 January 2023)

We theoretically calculate the density dynamic structure factor of one-dimensional Fermi superfluid with Raman-type spin-orbit coupling, and analyze its main dynamical character during phase transition between Bardeen-Cooper-Schrieffer superfluid and topological superfluid. Our theoretical results display four kinds of single-particle excitations induced by the two-branch structure of the single-particle spectrum, and the cross single-particle excitation is much easier to see in the spin dynamic structure factor at a small transferred momentum. Also we find a new rotonlike collective mode emerges at a fixed transferred momentum $q \simeq 2k_F$, and it only appears once the system enters the topological superfluid state. The occurrence of this rotonlike excitation is related to the switch of the global minimum in the single-particle spectrum from $k = 0$ to $k \simeq 2k_F$.

DOI: [10.1103/PhysRevA.107.013304](https://doi.org/10.1103/PhysRevA.107.013304)**I. INTRODUCTION**

Since the experimental realization of the spin-orbit coupling (SOC) effect in ultracold atomic gases [1–3], it has been possible to investigate many interesting and exotic matter states, such as the stripe phase [4], the topological state [5], etc., in this highly controllable system. To study properties of these many-body matter states, lots of scattering techniques based on the interplay between atoms and light play significant roles in enriching knowledge about them. For example, radio frequency can often be used to study the single-particle spectral function [6], while the two-photon Bragg scattering technique is utilized to study both single-particle excitations and rich collective ones [7,8].

As a many-body physical quantity, the dynamic structure factor is related to the imaginary part of the response function after Fourier transformation [9]. The definition of the dynamic structure factor is related closely to a certain physical operator, which is applied to perturb the system. Usually we focus our discussion on density operators of two spin components, which at the same time can impart a set of momentum and energy to the system to induce a density response. This density-related dynamic structure factor provides rich information about the dynamics of the system. At a small transferred momentum, the signal of the dynamic structure factor is dominated by all possible collective excitations, such as Goldstone phonon excitation [8], second sound [10], Leggett excitation [11–13], and possible Higgs excitation [14,15]. At a large transferred momentum, the dynamic structure factor is mainly influenced by the single-particle excitation [16],

which is determined by the many-body single-particle spectrum. Collecting all possible dynamical excitations displayed by dynamic structure factor, we can effectively understand dynamical properties related to a certain many-body matter state of the system. Usually the experimental measurement of many-body physical quantities is a challenging work. However, it is known that the density dynamic structure factor is proportional to the value of center-of-mass velocity of the system [17], which makes it feasible to measure density structure factor by a two-photon Bragg scattering experiment.

In this paper, we theoretically investigate one-dimensional (1D) Fermi superfluid with Raman-type SOC effect. The system can be realized by confining the motion of the system in the other two dimensions with the optical lattice technique. The physics we find in this paper is also expected to be valid in other systems, such as the nanowire setting in condensed matter physics [18]. This system has been found to experience a phase transition from a conventional Bardeen-Cooper-Schrieffer (BCS) superfluid to an interesting topological superfluid by continuously increasing an effective Zeeman field [5,19,20]. When the system comes into this topological superfluid, an impurity, a boundary or a topological defect can generate local Majorana fermions accompanied by a zero eigenenergy [21–23]. Since there is no symmetry breaking during phase transition, experimentally it is a great challenge to distinguish these two matter states. In this paper, we theoretically calculate the density dynamic structure factor of a 1D Raman–SOC Fermi superfluid with the random phase approximation [24], and analyze its main dynamical characteristics in both BCS and topological superfluids, which is expected to provide some dynamical information to understand and distinguish these two states.

This paper is organized as follows. In the next section, we will use the language of Green's function to introduce the microscopic model of a 1D Fermi superfluid with the Raman

*hszhao@qdu.edu.cn

†pengshigu@wipm.ac.cn

‡phy.zoupeng@gmail.com

SOC effect, outline the mean-field approximation, and show how to calculate the response function with the random phase approximation. We give results of the dynamic structure factor of both BCS and topological superfluids in Sec. III. In Sec. IV we give our conclusions. Some calculation details will be given in the Appendix.

II. METHODS

A. Model and Hamiltonian

For a two-spin-component 1D Raman–SOC Fermi superfluid with s -wave contact interaction, the system can be described by a model Hamiltonian,

$$H = \sum_{\sigma} \int dx \psi_{\sigma}^{\dagger}(x) \left[-\frac{1}{2m} \frac{\partial^2}{\partial x^2} - \mu \right] \psi_{\sigma}(x) - h \int dx [\psi_{\uparrow}^{\dagger}(x) e^{i2k_R x} \psi_{\downarrow}(x) + \text{H.c.}] + g_{1D} \int dx \psi_{\uparrow}^{\dagger}(x) \psi_{\downarrow}^{\dagger}(x) \psi_{\downarrow}(x) \psi_{\uparrow}(x), \quad (1)$$

where ψ_{σ} (ψ_{σ}^{\dagger}) is the annihilation (generation) operator of real particles with mass m for the spin- σ component and chemical potential μ . A dimensionless parameter $\gamma = -mg_{1D}/n_0$ is usually used to describe the strength of an attractive interaction g_{1D} of a uniform system at a bulk density n_0 , by which we can define the Fermi wave vector $k_F = \pi n_0/2$ and Fermi energy $E_F = k_F^2/2m$. h comes from the Rabi frequency of SOC interaction and is often defined as an effective Zeeman field, and k_R is the recoil momentum of the SOC laser beam, both of which come from the SOC effect. Here and in the following, we have set $\hbar = k_B = 1$ for simplicity. In many related references about the SOC effect, a further unitary transformation is carried out on the above Hamiltonian [21], which results in a term $\hat{k} \cdot \sigma$ that will appear in the single-particle Hamiltonian (σ is Pauli matrix), and the same operation also changes the physical meaning of spin index. So here we do not carry out this transformation to keep the original definition of spin index.

A standard mean-field treatment is done to the interaction Hamiltonian $H_{\text{int}} = g_{1D} \int dx \psi_{\uparrow}^{\dagger} \psi_{\downarrow}^{\dagger} \psi_{\downarrow} \psi_{\uparrow}$ with the usual definition of order parameter $\Delta = -g_{1D} \langle \psi_{\downarrow} \psi_{\uparrow} \rangle$. After Fourier transformation to the mean-field Hamiltonian, we can obtain its expression in the momentum representation, which reads

$$H_{\text{mf}} = \sum_{k\sigma} \xi_k c_{k\sigma}^{\dagger} c_{k\sigma} - h (c_{k+k_R\uparrow}^{\dagger} c_{k-k_R\downarrow} + \text{H.c.}) - \sum_k [\Delta c_{k\uparrow}^{\dagger} c_{-k\downarrow}^{\dagger} + \Delta^* c_{-k\downarrow} c_{k\uparrow}] \quad (2)$$

with $\xi_k = k^2/2m - \mu$. Usually the order parameter Δ is a complex number. However U(1) symmetry is broken in the ground state of the system, and the phase of Δ is randomly chosen as a constant number. Here we can just take this phase to be zero, and set $\Delta = \Delta^*$.

The exact diagonalization of mean-field Hamiltonian H_{mf} is a feasible but tedious task because of the long expression of each eigenvector. Luckily this problem can be solved by the motion equation of Green's function

$\omega \langle \langle c_1 | c_2 \rangle \rangle = \langle [c_1, c_2]_+ \rangle + \langle \langle [c_1, H_{\text{mf}}] | c_2 \rangle \rangle$, where c_1 and c_2 are any possible fermionic operators of the system, and the double-bracket notation $\langle \langle c_1 | c_2 \rangle \rangle$ is the corresponding momentum-energy Fourier transformation of space-time Green's function $-\langle T \psi_1(r_1, \tau) \psi_2(r_2, 0) \rangle$. Finally we find that the system has six independent Green's functions, which are

$$G_1(k, \omega) \equiv \langle \langle c_{k+k_R\uparrow} | c_{k+k_R\uparrow}^{\dagger} \rangle \rangle = \sum_l [G_1]_k^l / (\omega - E_k^l),$$

$$G_2(k, \omega) \equiv \langle \langle c_{k-k_R\downarrow} | c_{k-k_R\downarrow}^{\dagger} \rangle \rangle = \sum_l [G_2]_k^l / (\omega - E_k^l),$$

$$\Gamma(k, \omega) \equiv \langle \langle c_{k+k_R\uparrow} | c_{k-k_R\downarrow} \rangle \rangle = \sum_l [\Gamma]_k^l / (\omega - E_k^l),$$

$$S(k, \omega) \equiv \langle \langle c_{k-k_R\downarrow} | c_{k+k_R\uparrow}^{\dagger} \rangle \rangle = \sum_l [S]_k^l / (\omega - E_k^l),$$

$$F_1(k, \omega) \equiv \langle \langle c_{k+k_R\uparrow} | c_{-k+k_R\uparrow} \rangle \rangle = \sum_l [F_1]_k^l / (\omega - E_k^l),$$

$$F_2(k, \omega) \equiv \langle \langle c_{k-k_R\downarrow} | c_{-k-k_R\downarrow} \rangle \rangle = \sum_l [F_2]_k^l / (\omega - E_k^l), \quad (3)$$

where $l = \pm 1, \pm 2$ denotes respectively all four quasi-particle energy spectra $E_k^{(+1)} = -E_k^{(-1)} = U_k$ and $E_k^{(+2)} = -E_k^{(-2)} = D_k$. Symbols U_k and D_k are the up and down-branch quasiparticle spectra, respectively,

$$U_k = \sqrt{E_k^2 + h^2 + k^2 \lambda^2 + 2\sqrt{E_k^2 h^2 + \tilde{\xi}_k^2 k^2 \lambda^2}}, \quad (4)$$

$$D_k = \sqrt{E_k^2 + h^2 + k^2 \lambda^2 - 2\sqrt{E_k^2 h^2 + \tilde{\xi}_k^2 k^2 \lambda^2}}, \quad (5)$$

with $\tilde{\xi}_k = \xi_k + E_R$, $\lambda = k_R/m$, $E_R = k_R^2/2m$, and $E_k = \sqrt{\tilde{\xi}_k^2 + \Delta^2}$. These single-particle spectra greatly influence the static and dynamical properties of the ground state. All expressions of $[G_1]_k^l$, $[G_2]_k^l$, $[\Gamma]_k^l$, $[S]_k^l$, $[F_1]_k^l$, and $[F_2]_k^l$ will be listed in the Appendix. Based on the fluctuation and dissipation theorem, it is easy to get the relation between all physical quantities and corresponding Green's functions. For example, we obtain equations of density

$$n_1 = \sum_k \langle c_{k\uparrow}^{\dagger} c_{k\uparrow} \rangle = -\frac{1}{\pi} \sum_k \int d\omega \frac{\text{Im}[G_1(k, \omega)]}{e^{\omega/T} + 1}, \quad (6)$$

$$n_2 = \sum_k \langle c_{k\downarrow}^{\dagger} c_{k\downarrow} \rangle = -\frac{1}{\pi} \sum_k \int d\omega \frac{\text{Im}[G_2(k, \omega)]}{e^{\omega/T} + 1}, \quad (7)$$

and order parameter

$$\frac{\Delta}{g_{1D}} = -\sum_k \langle c_{-k\downarrow} c_{k\uparrow} \rangle = \frac{1}{\pi} \sum_k \int d\omega \frac{\text{Im}[\Gamma(k, \omega)]}{e^{\omega/T} + 1}, \quad (8)$$

with Green's functions G_1 , G_2 , and Γ in Eq. (3) at temperature T . By self-consistently solving the above density and order parameter equations, the value of chemical potential μ and order parameter Δ can be numerically calculated.

In the following, we take an interaction strength $\gamma = \pi$ and a typical experimental value of $k_R = 0.75k_F$. As shown in Fig. 1, the system experiences a phase transition from BCS superfluid to topological superfluid when increasing continuously the effective Zeeman field h over a critical value

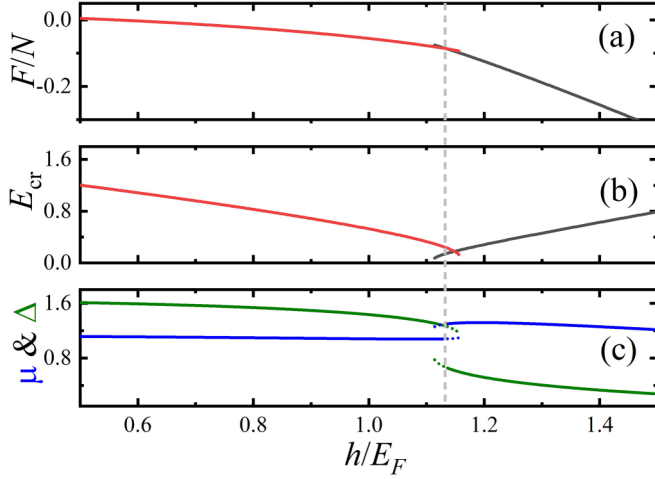


FIG. 1. The distribution of free energy in panel (a), $E_{\text{cr}} = |h - \sqrt{(\mu - E_R)^2 + \Delta^2}|$ in panel (b), and chemical potential (blue solid line) and order parameter (olive dashed line) at different effective Zeeman fields h during the phase transition between BCS superfluid (red solid line) and topological superfluid (black solid line). A gray dotted line marks the location of critical value of effective Zeeman magnetic field $h_c = 1.135E_F$ at $\gamma = \pi$ and $k_R = 0.75k_F$.

$h_c = 1.135E_F$, at which the free energies of two states are equal [see panel (a)]. This is a first-order phase transition, during which these two states compete with each other and make chemical potential μ and order parameter Δ experience a discontinuous variation at h_c [see panel (c)]. It should be noticed that the critical Zeeman field h_c here is larger than the another critical value of Zeeman field h at which the topological superfluid just turn out and $E_{\text{cr}} = |h - \sqrt{(\mu - E_R)^2 + \Delta^2}|$ just touches zero [see panel (b)].

The physical origin of this phase transition can also be understood from the geometrical structure of the down-branch single-particle spectrum D_k . As shown in Fig. 2, the global minimum of D_k experiences a switch from $k = 0$ (red dotted line) to a nonzero k (black solid line), when continuously in-

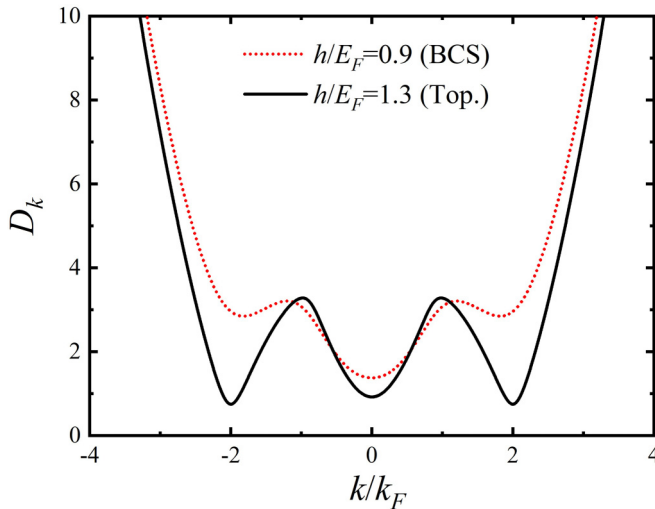


FIG. 2. The distribution of down-branch single-particle spectrum D_k at $\gamma = \pi$ and $k_R = 0.75k_F$.

creasing Zeeman field h . At the critical point ($h_c = 1.135E_F$), there are two options of the matter state for atoms to stay in the momentum space, in which the value of chemical potential [panel (c) of Fig. 1] can push all atoms to stay in the regime around $k = 0$, or both $k = 0$ and nonzero k minimum. The competition between these two situations generates both BCS and topological superfluid with the same free energy, and finally makes the system undergo this phase transition.

Next we will discuss the dynamical properties of the system and numerical methods to calculate them.

B. Response function and random phase approximation

In the Fermi superfluid, there are four different densities, which are denoted respectively by $n_1 = \sum_k \langle c_{k\uparrow}^\dagger c_{k\uparrow} \rangle$, $n_2 = \sum_k \langle c_{-k\downarrow}^\dagger c_{-k\downarrow} \rangle$, $n_3 = \sum_k \langle c_{-k\downarrow} c_{k\uparrow} \rangle$, and $n_4 = \sum_k \langle c_{k\uparrow}^\dagger c_{-k\downarrow}^\dagger \rangle$. n_1 and n_2 are the normal spin-up and spin-down densities, while n_3 and n_4 are anomalous densities (or superfluid correlation) [25]. Due to the interaction between particles, these densities are closely coupled with each other. Any fluctuation in each kind of density will make the other densities generate an obvious density fluctuation in them. This physics plays a significant role in the dynamical excitation of the system, and also demonstrates the importance and necessity of the term in the Hamiltonian beyond mean-field theory. The random phase approximation has been verified to be a good method to treat the fluctuation term of the Hamiltonian [24]. Comparing with experiments, it can even obtain some quantitatively reliable predictions in three-dimensional Fermi superfluid [26,27]. Its prediction also qualitatively agrees with quantum Monte Carlo data in a two-dimensional Fermi system [15]. Here we also use the same method to carry out a calculation to qualitatively study the dynamical excitation of 1D SOC Fermi superfluid. Its main idea is introduced in the following.

Following the standard linear response theorem, a weak external density perturbation potential $V_{\text{ext}} = [V_1, V_2, V_3, V_4]$, which carries a specific momentum q , is exerted on the Fermi superfluid. The corresponding perturbation Hamiltonian is described by $H_{\text{ext}} = \sum_{kq} \Psi_{k+q}^\dagger (V_1 \sigma_1 + V_2 \sigma_2 + V_3 \sigma_3 + V_4 \sigma_4) \Psi_k$. Here $\Psi_k = [c_{k\uparrow}, c_{-k\downarrow}^\dagger]^T$ is the field operator matrix in the momentum representation. Four matrices $\sigma_1 = (I + \sigma_z)/2$, $\sigma_2 = (I - \sigma_z)/2$, $\sigma_3 = (\sigma_x - i\sigma_y)/2$, and $\sigma_4 = (\sigma_x + i\sigma_y)/2$ are defined with Pauli matrices $\sigma_{x,y,z}$ and unit matrix I . This perturbation Hamiltonian H_{ext} will induce a density fluctuation of all densities, labeled by a matrix

$$\rho_q = \sum_k \begin{bmatrix} n_{kq}^1 \\ n_{kq}^2 \\ n_{kq}^3 \\ n_{kq}^4 \end{bmatrix} = \sum_k \begin{bmatrix} \Psi_k^\dagger \sigma_1 \Psi_{k+q} \\ \Psi_k^\dagger \sigma_2 \Psi_{k+q} \\ \Psi_k^\dagger \sigma_3 \Psi_{k+q} \\ \Psi_k^\dagger \sigma_4 \Psi_{k+q} \end{bmatrix}. \quad (9)$$

These density fluctuations in reverse play a non-negligible role in generating a fluctuation Hamiltonian $H_{\text{sc}} = \sum_q \rho_q^\dagger A_q$, which is usually called the self-consistent dynamical potential [28]. Here

$$A_q = \begin{bmatrix} n_q^2 \\ n_q^1 \\ n_q^3 \\ n_q^4 \end{bmatrix} = g_{\text{1D}} \sum_k \begin{bmatrix} n_{kq}^2 \\ n_{kq}^1 \\ n_{kq}^3 \\ n_{kq}^4 \end{bmatrix}$$

is the strength of the fluctuation potential. Different from the two- or three-dimension case, the contribution from n_q^3 and n_q^4 is not divergent and there is no need to carry on renormalization to one-dimensional interaction strength g_{1D} [15,26].

In a weak perturbation situation, the amplitude of density fluctuation ρ_q is proportional to the external potential V_{ext} , and they are connected to each other by

$$\rho_q = \chi V_{\text{ext}}, \quad (10)$$

where χ is the response function of the system and includes rich information about the dynamical excitation, however, this calculation is usually quite hard to carry out. As discussed above, a feasible way to figure out this problem is to use the random phase approximation, which collects effects of both V_{ext} and $V_{\text{sf}} = M_I A_q$ to define an effective external potential

$$V_{\text{eff}} = V_{\text{ext}} + V_{\text{sf}}. \quad (11)$$

Then the motion of real gases in external potential V_{ext} is equivalent to the motion of mean-field gases in this effective potential V_{eff} . So the density fluctuation is connected to this effective potential V_{eff} by

$$\rho_q = \chi^0 V_{\text{eff}}, \quad (12)$$

where χ^0 is the response function in the mean-field approximation, whose calculation is relatively much easier. Finally, with Eqs. (9)–(12), we find χ and χ^0 are related to each other by the equation

$$\chi = \frac{\chi^0}{1 - \chi^0 M_I g_{1D}}, \quad (13)$$

where

$$M_I = \begin{bmatrix} 0 & 1 & 0 & 0 \\ 1 & 0 & 0 & 0 \\ 0 & 0 & 0 & 1 \\ 0 & 0 & 1 & 0 \end{bmatrix}$$

is a constant matrix reflecting the coupling situation of four different densities.

Next we discuss the derivation of the mean-field response function χ^0 , which is a 4×4 matrix:

$$\chi^0 = \begin{bmatrix} \chi_{11}^0 & \chi_{12}^0 & \chi_{13}^0 & \chi_{14}^0 \\ \chi_{21}^0 & \chi_{22}^0 & \chi_{23}^0 & \chi_{24}^0 \\ \chi_{31}^0 & \chi_{32}^0 & \chi_{33}^0 & \chi_{34}^0 \\ \chi_{41}^0 & \chi_{42}^0 & \chi_{43}^0 & \chi_{44}^0 \end{bmatrix}. \quad (14)$$

Here any matrix element $\chi_{ij}^0(x_1, x_2, \tau, 0) \equiv -\langle \hat{n}_i(x_1, \tau) \hat{n}_j(x_2, 0) \rangle$. In the uniform system, all response function should only be a function of relative coordinate $x = x_1 - x_2$ and imaginary time τ . So a generalized coordinate $R = (x, \tau)$ is used to continue the discussion. Based on Wick's theorem, we should consider all possible two-operator contraction terms, which are all related to the six independent Green's functions (3). We find that the mean-field response function can be displayed by $\chi^0 = A + B$, in which A is the mean-field response function connecting to Green's functions G_1 , G_2 , and Γ , while B connects the SOC Green's functions S , F_1 , and F_2 . For example, in the spatial and time representation,

$$\chi_{11}^0(R) \equiv -\langle \hat{n}_1(x_1, \tau) \hat{n}_1(x_2, 0) \rangle = A_{11}(R) + B_{11}(R),$$

where $A_{11}(R) = G_1(-R)G_1(R)$ and $B_{11}(R) = F_1^\dagger(-R)F_1(R)$. In the ground state ($\Delta = \Delta^*$), we find $F_1^\dagger = F_1$. After Fourier transformation to Green's functions and with identical relation $\frac{1}{\beta} \sum_{ip_n} \frac{1}{ip_n - \varepsilon} \times \frac{1}{ip_n + iq_n - \varepsilon'} = \frac{f(\varepsilon) - f(\varepsilon')}{iq_n + \varepsilon - \varepsilon'}$ (ip_n and iq_n are Matsubara frequencies, and $f(x)$ is the Fermi distribution function), we obtain the expression of all matrix elements in the momentum-energy representation

$$\chi^0(q, \omega) = A(q, \omega) + B(q, \omega), \quad (15)$$

where

$$A = \begin{bmatrix} A_{11} & A_{12} & A_{13} & A_{14} \\ A_{12} & A_{22} & A_{23} & A_{24} \\ A_{14} & A_{24} & -A_{12} & A_{34} \\ A_{13} & A_{23} & A_{43} & -A_{12} \end{bmatrix}$$

has nine independent matrix elements and

$$B = \begin{bmatrix} B_{11} & B_{12} & B_{13} & B_{14} \\ B_{12} & B_{22} & B_{23} & B_{24} \\ B_{14} & B_{24} & B_{33} & B_{34} \\ B_{13} & B_{23} & B_{43} & B_{33} \end{bmatrix}$$

has ten independent matrix elements. All expressions of these matrix elements are listed in the Appendix.

C. Dynamic structure factor

With Eqs. (13) and (15), we get expressions of both the density and spin response functions, which are expressed by

$$\chi_n \equiv \chi_{11} + \chi_{22} + \chi_{12} + \chi_{21}, \quad (16)$$

$$\chi_s \equiv \chi_{11} + \chi_{22} - \chi_{12} - \chi_{21}.$$

And the density dynamic structure factor $S_n(q, \omega)$ and the spin one $S_s(q, \omega)$ are connected with the corresponding response function by

$$S_{n/s} = -\frac{1}{\pi} \frac{1}{1 - e^{-\omega/T}} \text{Im}[\chi_{n/s}], \quad (17)$$

where q and ω are the transferred momentum and energy, respectively. The sum rules of these two dynamic structure factors were introduced in the Ref. [29].

III. RESULTS

In the following discussions, we still focus on the interaction strength $\gamma = \pi$ and also the recoil momentum $k_R = 0.75k_F$ at zero temperature. These parameters are the same as the ones in Fig. 1. We numerically calculate the density and spin dynamic structure factor, which are shown in Figs. 3 and 4, respectively, in the phase transition between BCS superfluid (upper two panels) and topological superfluid (lower two panels). Generally we investigate a full dynamical excitation in different transferred momenta q , including the low energy (or momentum) collective excitation to the high energy (or momentum) single-particle excitation. Of course, the presence of SOC effect goes on enriching dynamical behaviors compared to those in conventional Fermi superfluid.

A. Collective phonon and rotonlike excitations

At a low transferred energy ω , it is easy to investigate the collective excitation. By continuously increasing transferred

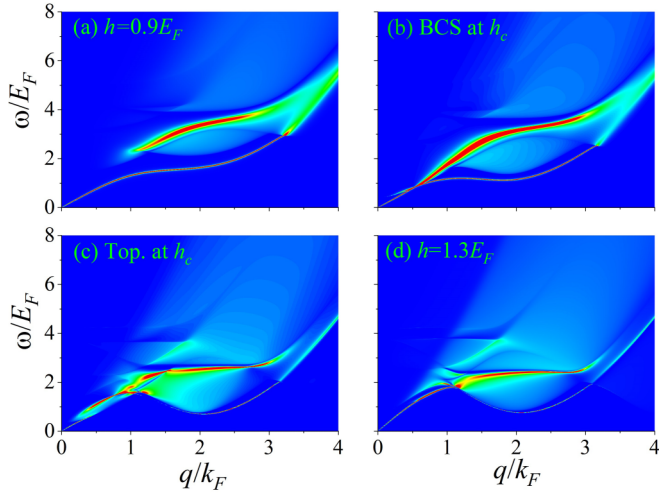


FIG. 3. The density dynamic structure factor $S_n(q, \omega)$ of the SOC Fermi superfluid at different Zeeman fields $h = 0.9E_F, h_c, 1.3E_F$. Panels (a) and (b) shows results in BCS superfluid, while panels (c) and (d) show results in topological superfluid.

momentum q from zero, we initially see a gapless phonon excitation in the density dynamic structure factor $S_n(q, \omega)$, which is shown by the lower red curve in all four panels of Fig. 3. When the system is in the BCS superfluid ($h \leq h_c$, upper two panels), the spectrum of collective phonon excitation just monotonically rises with transferred momentum q , and finally merges into the single-particle excitation continuum at a certain large enough q . In the whole BCS regime, the phonon velocity almost does not vary much with the effective Zeeman field h , except in a narrow regime close to transition where BCS superfluid becomes a metastable state and the velocity suddenly drops (red solid and dotted lines of Fig. 5). Of course, the gapless phonon excitation can also be seen in the topological superfluid (black solid and dot line of Fig. 5), and its velocity monotonically increases with Zeeman field

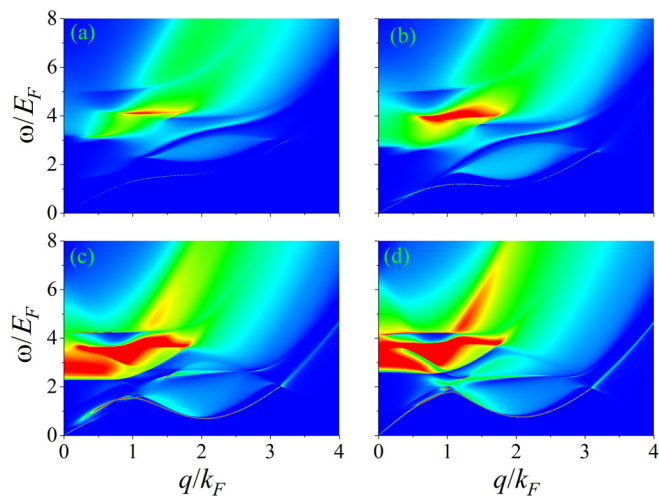


FIG. 4. The spin dynamic structure factor $S_s(q, \omega)$ of the SOC Fermi superfluid at different Zeeman fields $h = 0.9E_F, h_c, 1.3E_F$. The arrangement of parameters in these four panels is the same as that in Fig. 3.

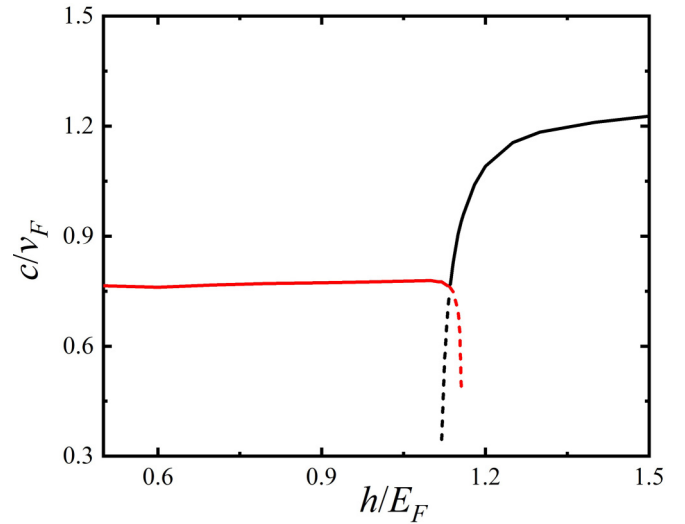


FIG. 5. The sound velocity c at different effective Zeeman fields h .

h and finally saturates to a constant value. In the critical regime $h = h_c$, the BCS and topological states have the same Free energy. Although we calculate respectively their dynamic structure factor, the phonon excitation of one state may be potentially influenced by the other, and turns out to be a complex excitation behavior (see Fig. 3 and 4).

Besides the phonon collective excitation, we investigate a new collective rotonlike excitation only appearing in the topological superfluid. As shown in the lower two panels of both Figs. 3 and 4, this rotonlike excitation is a natural extension of the phonon mode, and it is denoted by a local minimum of the excitation spectrum at a fixed momentum $q \simeq 2k_F$, which is just the global minimum of the down-branch spectrum D_k (see the red line of Fig. 2). There is no rotonlike excitation in the BCS superfluid, where $q \simeq 2k_F$ is just a local minimum and the global minimum is located at $q = 0$. These results tell us that the emergence of rotonlike excitation is closely related to the formation of the global minimum at $q \simeq 2k_F$, which is just the character of spectrum D_k in topological superfluid. All discussions above hint that the specific single-particle effect brought about by the SOC effect plays an important role in the appearance of the rotonlike excitation at a certain interaction strength. In general, we have also checked that the same rotonlike mode can be seen in other different interaction strengths (for example $\gamma = 2.5, 4.0$) and recoil momentum k_R , and the location of the rotonlike excitation is always fixed at $q \simeq 2k_F$.

The dynamical behavior of collective mode can be displayed by both the density and spin dynamic structure factor. However a different excitation related to single-particle excitation happens at a relatively large transferred energy ω when q is small, whose physical origin will be introduced in the following.

B. Threshold of single-particle excitation spectrum

When the transferred energy ω is large enough, a pair breaking of Cooper pairs will occur and separate pairs into free Fermi atoms. Indeed a great part of the dynamical excitation in Figs. 3 and 4 is dominated by this pair-breaking

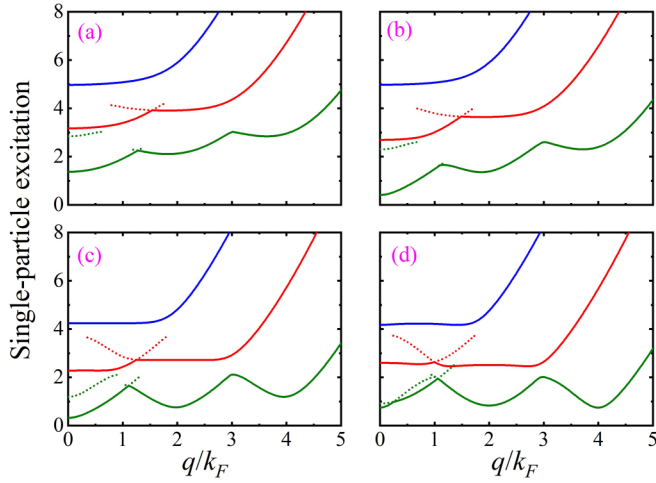


FIG. 6. Four kinds of single-particle excitation spectra. Olive line: $D_k \leftrightarrow D_{k+q}$. Red line: $D_k \leftrightarrow U_{k+q}$ and $U_k \leftrightarrow D_{k+q}$. Blue line: $U_k \leftrightarrow U_{k+q}$. The arrangement of parameters in these four panels is the same as that in Fig. 3.

effect. In the density dynamic structure factor S_n , this effect usually is very obvious in a relatively large transferred momentum $q > k_F$, where the collective excitations are very suppressed. Differently from the conventional Fermi superfluid, this single-particle excitation takes up a large regime in the spin dynamic structure factor S_s , even for a small or zero transferred momentum q . Before understanding this single-particle excitation, it is necessary to study the threshold energy to break a Cooper pair.

This pair-breaking excitation is related to the two-branch structure of quasiparticle spectra U_k and D_k , and the two atoms forming a Cooper-pair can come from the same or different single-particle spectra. This two-branch structure of the spectrum generates much richer single-particle excitation than the conventional Fermi superfluid, and induces four possible combinations of Fermi atoms in a Cooper pair, namely the DD , DU , UD , and UU types. The minimum energy at a certain momentum q to break a pair should be $\min[D_k + D_{k+q}]$, $\min[D_k + U_{k+q}]$, $\min[U_k + D_{k+q}]$, or $\min[U_k + U_{k+q}]$. Also due to the three-potential-well geometry of down-branch spectrum D_k , there are not only the global minimum energy but also many possible local minima to break a Cooper pair in single-particle excitations. These results are shown in Fig. 6. The lowest olive line denotes the DD excitation, and its minimum value of pair-breaking excitation is from the down-branch quasiparticle spectrum ($\min[D_k + D_{k+q}]$). Besides the global minimum, it also has two or even three local minima at some specific transferred momentum q , displayed by olive dotted lines. In other regimes of q , these local minima will disappear since the geometry of the spectrum has been changed. From the BCS superfluid ($h = 0.9E_F$) to the topological superfluid ($h = 1.3E_F$), the value of order parameter Δ monotonically decreases with effective Zeeman field h [shown by panel (b) of Fig. 1]. This behavior makes the pair-breaking excitation much easier at large h , and generally makes the olive line become lower and lower.

The red line denotes DU and UD excitations, which are overlapped with each other. The two atoms in a pair comes

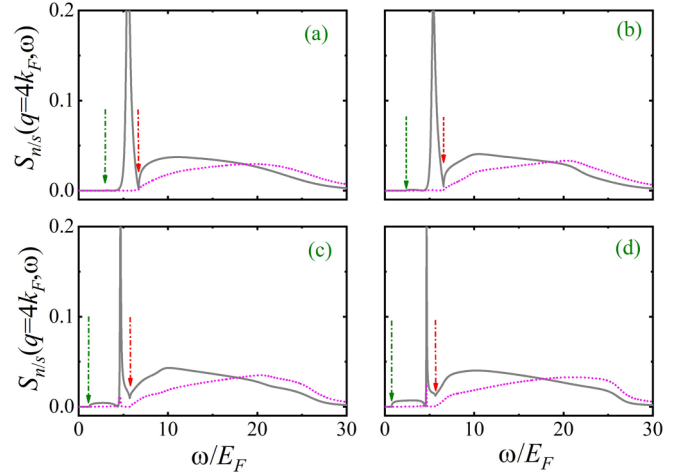


FIG. 7. The density (gray) and spin (magenta) dynamical structure factor of 1D SOC Fermi superfluid at transferred momentum $q = 4k_F$. The arrangement of parameters in these four panels is the same as that in Fig. 3.

from different branches of the spectrum. They start from $\min[D_k + U_{k+q}]$, whose energy is higher than the DD one. Similar to DD excitation, there are some possible local minima in these cross excitations. It should be emphasized that this DU single-particle excitation at a small q displays a much stronger excitation strength in the spin dynamic structure factor than the one in the density dynamic structure factor (see Fig. 4), which also reflects the coupling between different spin components.

Starting from $\min[U_k + U_{k+q}]$, the blue line is the UU excitation, which requires the largest excitation energy. This excitation has less density of state in the small q regime in the BCS superfluid, while the topological state enhances its density of state and displays a relatively stronger signal.

All of these kinds of critical single-particle excitations are located in the colorful edge curves of Figs. 3 and 4, and mark the regime of single-particle excitation. To better understand the dynamical excitation in these colorful panels, we will discuss the dynamic structure factor at a selected transferred momentum q .

C. Dynamic excitation at a constant momentum q

For a relatively large transferred momentum $q \gg k_F$, the dynamic structure factor will be dominated by the single-particle excitation. As shown in Fig. 7, we investigate the density and spin dynamic structure factor at $q = 4k_F$ in both BCS and topological superfluids. In all four panels, we can see two obvious single-particle excitations (DD and DU type) and a sharp collective phonon excitation. The locations of threshold energy for two single-particle excitations are respectively labeled by the olive and red dash-dot arrows. Here the phonon excitation has already been mixed with the DD single-particle excitation, which results in a nonzero expansion width of the peak of collective mode. Its location is between the olive and red arrows, after which more and more single-particle excitations result. There is no obvious UU excitation signal here, which is drowned into the background of other single-particle

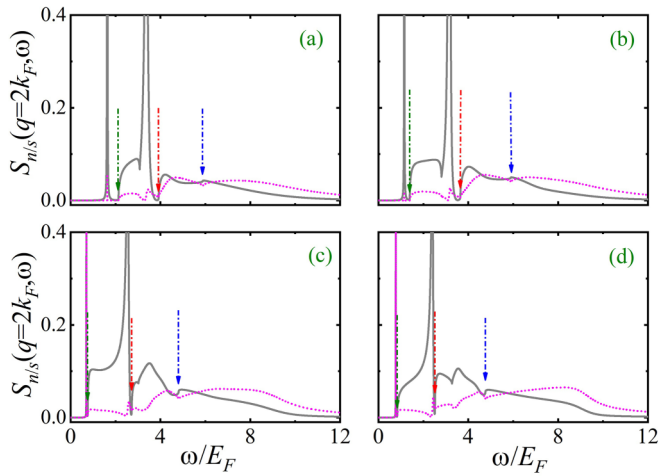


FIG. 8. The density (gray) and spin (magenta) dynamical structure factor of 1D SOC Fermi superfluid at transferred momentum $q = 2k_F$. The arrangement of parameters in these four panels is the same as that in Fig. 3.

excitations. At $q = 4k_F$, it is easy to see that the topological superfluid displays a relatively stronger DD excitation $q = 4k_F$ than the one in the BCS state.

When taking transferred momentum $q = 2k_F$, the competition between collective mode and single-particle mode is very intense. We see a much richer dynamical excitation. As shown in Fig. 8, both S_n and S_s present two sharp deltalike peaks and all three kinds of single-particle excitation, the threshold locations of which are still respectively labeled by olive, red, and blue arrows. At $q = 2k_F$, the left sharp peak in four panels locates on the left side of green arrows (DD type excitation). In fact it is a natural extension of the collective phonon excitation, which is close to merging into the single-particle excitation continuum. The peak in topological superfluid (lower two panels) happens at a relatively low excitation energy since the system generates a rotonlike collective excitation, which has been discussed above. Regarding the right sharp peak, it locates at the higher red “eyebrow” position in Fig. 3; its physical origin is still an open question, and we argue that it may be the possible collective Higgs oscillation, which has totally merged into the single-particle excitation [30].

For a much smaller transferred momentum $q = 1k_F$, the competition of all dynamical excitations displayed by two dynamic structure factors becomes much more intense, and the energy differences among all possible excitations are not far away from each other. The results for both BCS and topological states are shown in Fig. 9. When $h = 0.9E_F$ (BCS), we see one clear phonon excitation around $\omega \simeq 1.2E_F$, and all three other kinds of single-particle excitations to the right, whose initial excitation energies are marked by arrows. In this case, DU type excitation has two threshold energies. While the left red arrow is from the global minimum of excitation energy, $\min[D_k + U_{k+q}]$, the right one comes from its local minimum. Similar physics is also found for $h = h_c$ (BCS side). However a high peak ($\omega \simeq 2.3E_F$) rises after the olive arrows. When the system comes into the topological regime ($h = 1.3E_F$), this unknown peak ($\omega \simeq 1.9E_F$) will present a deltalike excitation

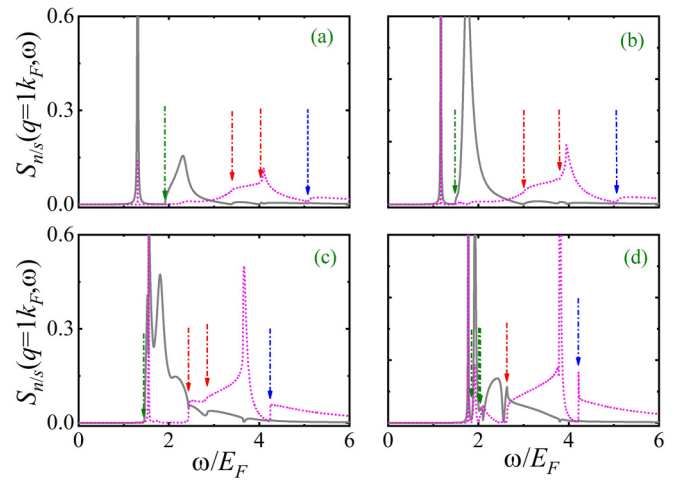


FIG. 9. The density (blue) and spin (red) dynamical structure factor of 1D SOC Fermi superfluid at transferred momentum $q = 1k_F$. The arrangement of parameters in these four panels is the same as that in Fig. 3.

in a certain narrow energy regime (see also the lower right panel of Fig. 3). It seems that this unknown peak is different from the unknown one discussed above. Maybe it is generated by the competition of two collective modes in two different states, and we argue it is the redundancy of collective modes in the metastable state. Regarding the single-particle excitation, three minima of DD type have also been obtained in this case, and their positions are located by three olive arrows, each of which will induce the regular oscillation of the curve of the dynamic structure factor.

IV. CONCLUSIONS AND OUTLOOK

In summary, we numerically calculate the density and spin dynamic structure factor of 1D Raman–SOC Fermi superfluid with the random phase approximation during the phase transition between BCS and topological superfluid. The dynamic structure factor presents rich single-particle excitations and collective mode. Due to the two-branch structure of the single-particle spectrum, there are three kinds of single-particle excitation, namely DD , DU (UD), and UU excitation. We also calculate their own threshold energies to break a Cooper pair. Among these single-particle excitations, the DU one takes a great part only in the spin dynamic structure factor at a small transferred momentum, which comes from the coupling effect between spin and orbital motion. Regarding collective excitation, there is an interesting rotonlike collective excitation at $k \simeq 2k_F$ when the system comes into the topological state. The generation of this rotonlike excitation is due to the switch of the global minimum of the single-particle spectrum D_k from $k = 0$ to $k \simeq 2k_F$. Similar physics has also been found in other different interaction strengths γ and recoil momenta k_R . Also these are some unknown quasi-delta-like excitations when q is between k_F and $2k_F$, whose physical origin is worth explaining in our future research. Also it will be interesting to investigate the Majorana mode in the future in a system with a hard-wall boundary condition or a system

with a soliton, which is absent in the system we consider in this paper.

ACKNOWLEDGMENTS

We are grateful for fruitful discussions with Hui Hu, Wei Yi, and Wei Zhang. This research was supported by the National Natural Science Foundation of China, Grants No. 11804177 (P.Z.), No. 11547034 (H.Z.), and No. 11974384 (S.-G.P.).

APPENDIX

In this Appendix, we will list expressions of six independent Green' functions and mean-field response functions $\chi^0 = A + B$:

$$G_1(k, \omega) = \sum_l [G_1]_k^l / (\omega - E_k^l), \text{ with}$$

$$\begin{aligned} [G_1]_k^1 &= + \frac{U_k^2 - \xi_-^2 - h^2 - \Delta^2}{2(U_k^2 - D_k^2)} \\ &+ \frac{\xi_+ U_k^2 - \xi_+ \xi_-^2 + \xi_- h^2 - \xi_+ \Delta^2}{2U_k(U_k^2 - D_k^2)}, \\ [G_1]_k^2 &= + \frac{U_k^2 - \xi_-^2 - h^2 - \Delta^2}{2(U_k^2 - D_k^2)} \\ &- \frac{\xi_+ U_k^2 - \xi_+ \xi_-^2 + \xi_- h^2 - \xi_+ \Delta^2}{2U_k(U_k^2 - D_k^2)}, \\ [G_1]_k^3 &= - \frac{D_k^2 - \xi_-^2 - h^2 - \Delta^2}{2(U_k^2 - D_k^2)} \\ &- \frac{\xi_+ D_k^2 - \xi_+ \xi_-^2 + \xi_- h^2 - \xi_+ \Delta^2}{2D_k(U_k^2 - D_k^2)}, \\ [G_1]_k^4 &= - \frac{D_k^2 - \xi_-^2 - h^2 - \Delta^2}{2(U_k^2 - D_k^2)} \\ &+ \frac{\xi_+ D_k^2 - \xi_+ \xi_-^2 + \xi_- h^2 - \xi_+ \Delta^2}{2D_k(U_k^2 - D_k^2)}, \end{aligned}$$

where $\xi_{\pm} = (k \pm k_R)^2 / 2m - \mu$. $G_2(k, \omega) = \sum_l [G_2]_k^l / (\omega - E_k^l)$, with

$$\begin{aligned} [G_2]_k^1 &= + \frac{U_k^2 - \xi_+^2 - h^2 - \Delta^2}{2(U_k^2 - D_k^2)} \\ &+ \frac{\xi_- U_k^2 - \xi_- \xi_+^2 + \xi_+ h^2 - \xi_- \Delta^2}{2U_k(U_k^2 - D_k^2)}, \\ [G_2]_k^2 &= + \frac{U_k^2 - \xi_+^2 - h^2 - \Delta^2}{2(U_k^2 - D_k^2)} \\ &- \frac{\xi_- U_k^2 - \xi_- \xi_+^2 + \xi_+ h^2 - \xi_- \Delta^2}{2U_k(U_k^2 - D_k^2)}, \\ [G_2]_k^3 &= - \frac{D_k^2 - \xi_+^2 - h^2 - \Delta^2}{2(U_k^2 - D_k^2)} \\ &- \frac{\xi_- D_k^2 - \xi_- \xi_+^2 + \xi_+ h^2 - \xi_- \Delta^2}{2D_k(U_k^2 - D_k^2)}, \end{aligned}$$

$$\begin{aligned} [G_2]_k^4 &= - \frac{D_k^2 - \xi_+^2 - h^2 - \Delta^2}{2(U_k^2 - D_k^2)} \\ &+ \frac{\xi_- D_k^2 - \xi_- \xi_+^2 + \xi_+ h^2 - \xi_- \Delta^2}{2D_k(U_k^2 - D_k^2)}. \end{aligned}$$

$$\Gamma(k, \omega) = \sum_l [\Gamma]_k^l / (\omega - E_k^l), \text{ with}$$

$$\begin{aligned} [\Gamma]_k^1 &= -[\Gamma]_k^2 = - \frac{\Delta[U_k^2 - (\xi_-^2 - h^2 + \Delta^2)]}{2U_k(U_k^2 - D_k^2)}, \\ [\Gamma]_k^3 &= -[\Gamma]_k^4 = + \frac{\Delta[D_k^2 - (\xi_-^2 - h^2 + \Delta^2)]}{2D_k(U_k^2 - D_k^2)}. \end{aligned}$$

$$S(k, \omega) = \sum_l [S]_k^l / (\omega - E_k^l), \text{ with}$$

$$\begin{aligned} [S]_k^1 &= h \left[- \frac{\xi_+ + \xi_-}{2(U_k^2 - D_k^2)} - \frac{U_k^2 + \xi_+ \xi_- - h^2 + \Delta^2}{2U_k(U_k^2 - D_k^2)} \right], \\ [S]_k^2 &= h \left[- \frac{\xi_+ + \xi_-}{2(U_k^2 - D_k^2)} + \frac{U_k^2 + \xi_+ \xi_- - h^2 + \Delta^2}{2U_k(U_k^2 - D_k^2)} \right], \\ [S]_k^3 &= h \left[+ \frac{\xi_+ + \xi_-}{2(U_k^2 - D_k^2)} + \frac{D_k^2 + \xi_+ \xi_- - h^2 + \Delta^2}{2D_k(U_k^2 - D_k^2)} \right], \\ [S]_k^4 &= h \left[+ \frac{\xi_+ + \xi_-}{2(U_k^2 - D_k^2)} - \frac{D_k^2 + \xi_+ \xi_- - h^2 + \Delta^2}{2D_k(U_k^2 - D_k^2)} \right]. \end{aligned}$$

$$F_1(k, \omega) = \sum_l [F_1]_k^l / (\omega - E_k^l), \text{ with}$$

$$\begin{aligned} [F_1]_k^1 &= - \frac{\Delta h(2U_k + \xi_+ - \xi_-)}{2U_k(U_k^2 - D_k^2)}, \\ [F_1]_k^2 &= - \frac{\Delta h(2U_k - \xi_+ + \xi_-)}{2U_k(U_k^2 - D_k^2)}, \\ [F_1]_k^3 &= + \frac{\Delta h(2D_k + \xi_+ - \xi_-)}{2D_k(U_k^2 - D_k^2)}, \\ [F_1]_k^4 &= + \frac{\Delta h(2D_k - \xi_+ + \xi_-)}{2D_k(U_k^2 - D_k^2)}. \end{aligned}$$

$$F_2(k, \omega) = \sum_l [F_2]_k^l / (\omega - E_k^l), \text{ with}$$

$$\begin{aligned} [F_2]_k^1 &= + \frac{\Delta h(2U_k - \xi_+ + \xi_-)}{2U_k(U_k^2 - D_k^2)}, \\ [F_2]_k^2 &= + \frac{\Delta h(2U_k + \xi_+ - \xi_-)}{2U_k(U_k^2 - D_k^2)}, \\ [F_2]_k^3 &= - \frac{\Delta h(2D_k - \xi_+ + \xi_-)}{2D_k(U_k^2 - D_k^2)}, \\ [F_2]_k^4 &= - \frac{\Delta h(2D_k + \xi_+ - \xi_-)}{2D_k(U_k^2 - D_k^2)}. \end{aligned}$$

The expressions of all nine independent matrix elements in mean-field response function A are

$$\begin{aligned}
 A_{11} &= + \sum_{pl'} [G_1]_p^l [G_1]_{p+q}^{l'} \frac{f(E_p^l) - f(E_{p+q}^{l'})}{i\omega_n + E_p^l - E_{p+q}^{l'}}, \\
 A_{12} &= - \sum_{pl'} [\Gamma]_p^l [\Gamma]_{p+q}^{l'} \frac{f(E_p^l) - f(E_{p+q}^{l'})}{i\omega_n + E_p^l - E_{p+q}^{l'}}, \\
 A_{13} &= + \sum_{pl'} [G_1]_p^l [\Gamma]_{p+q}^{l'} \frac{f(E_p^l) - f(E_{p+q}^{l'})}{i\omega_n + E_p^l - E_{p+q}^{l'}}, \\
 A_{14} &= + \sum_{pl'} [\Gamma]_p^l [G_1]_{p+q}^{l'} \frac{f(E_p^l) - f(E_{p+q}^{l'})}{i\omega_n + E_p^l - E_{p+q}^{l'}}, \\
 A_{22} &= + \sum_{pl'} [G_2]_p^l [G_2]_{p+q}^{l'} \frac{f(E_p^l) - f(E_{p+q}^{l'})}{i\omega_n + E_p^l - E_{p+q}^{l'}}, \\
 A_{23} &= - \sum_{pl'} [\Gamma]_p^l [G_1]_{p+q}^{l'} \frac{f(E_p^l) - f(E_{p+q}^{l'})}{i\omega_n + E_p^l - E_{p+q}^{l'}}, \\
 A_{24} &= - \sum_{pl'} [G_1]_p^{-l} [\Gamma]_{p+q}^{l'} \frac{f(E_p^l) - f(E_{p+q}^{l'})}{i\omega_n + E_p^l - E_{p+q}^{l'}}, \\
 A_{34} &= + \sum_{pl'} [G_2]_p^{-l} [G_2]_{p+q}^{l'} \frac{f(E_p^l) - f(E_{p+q}^{l'})}{i\omega_n + E_p^l - E_{p+q}^{l'}}, \\
 A_{43} &= + \sum_{pl'} [G_1]_p^l [G_1]_{p+q}^{-l'} \frac{f(E_p^l) - f(E_{p+q}^{l'})}{i\omega_n + E_p^l - E_{p+q}^{l'}},
 \end{aligned}$$

where $f(x) = 1/(e^{x/k_B T} + 1)$ is the Fermi-Dirac distribution function. The expressions of ten independent matrix elements

in mean-field response function B are

$$\begin{aligned}
 B_{11} &= - \sum_{pl'} [F_1]_p^l [F_1]_{p+q}^{l'} \frac{f(E_p^l) - f(E_{p+q}^{l'})}{i\omega_n + E_p^l - E_{p+q}^{l'}}, \\
 B_{12} &= + \sum_{pl'} [S]_p^l [S]_{p+q}^{l'} \frac{f(E_p^l) - f(E_{p+q}^{l'})}{i\omega_n + E_p^l - E_{p+q}^{l'}}, \\
 B_{13} &= - \sum_{pl'} [S]_p^l [F_1]_{p+q}^{l'} \frac{f(E_p^l) - f(E_{p+q}^{l'})}{i\omega_n + E_p^l - E_{p+q}^{l'}}, \\
 B_{14} &= - \sum_{pl'} [F_1]_p^l [S]_{p+q}^{l'} \frac{f(E_p^l) - f(E_{p+q}^{l'})}{i\omega_n + E_p^l - E_{p+q}^{l'}}, \\
 B_{22} &= - \sum_{pl'} [F_2]_p^l [F_2]_{p+q}^{l'} \frac{f(E_p^l) - f(E_{p+q}^{l'})}{i\omega_n + E_p^l - E_{p+q}^{l'}}, \\
 B_{23} &= + \sum_{pl'} [S]_p^l [F_2]_{p+q}^{l'} \frac{f(E_p^l) - f(E_{p+q}^{l'})}{i\omega_n + E_p^l - E_{p+q}^{l'}}, \\
 B_{24} &= + \sum_{pl'} [F_2]_p^l [S]_{p+q}^{l'} \frac{f(E_p^l) - f(E_{p+q}^{l'})}{i\omega_n + E_p^l - E_{p+q}^{l'}}, \\
 B_{33} &= - \sum_{pl'} [F_2]_p^l [F_1]_{p+q}^{l'} \frac{f(E_p^l) - f(E_{p+q}^{l'})}{i\omega_n + E_p^l - E_{p+q}^{l'}}, \\
 B_{34} &= - \sum_{pl'} [S]_p^{-l} [S]_{p+q}^{l'} \frac{f(E_p^l) - f(E_{p+q}^{l'})}{i\omega_n + E_p^l - E_{p+q}^{l'}}, \\
 B_{43} &= - \sum_{pl'} [S]_p^l [S]_{p+q}^{-l'} \frac{f(E_p^l) - f(E_{p+q}^{l'})}{i\omega_n + E_p^l - E_{p+q}^{l'}}.
 \end{aligned}$$

-
- [1] Y.-J. Lin, K. Jiménez-García, and I. B. Spielman, Spin-orbit-coupled Bose-Einstein condensates, *Nature (London)* **471**, 83 (2011).
- [2] P. Wang, Z.-Q. Yu, Z. Fu, J. Miao, L. Huang, S. Chai, H. Zhai, and J. Zhang, Spin-Orbit Coupled Degenerate Fermi Gases, *Phys. Rev. Lett.* **109**, 095301 (2012).
- [3] L. W. Cheuk, A. T. Sommer, Z. Hadzibabic, T. Yefsah, W. S. Bakr, and M. W. Zwierlein, Spin-Injection Spectroscopy of a Spin-Orbit Coupled Fermi Gas, *Phys. Rev. Lett.* **109**, 095302 (2012).
- [4] T.-L. Ho and S. Zhang, Bose-Einstein Condensates with Spin-Orbit Interaction, *Phys. Rev. Lett.* **107**, 150403 (2011).
- [5] L. Jiang, T. Kitagawa, J. Alicea, A. R. Akhmerov, D. Pekker, G. Refael, J. Ignacio Cirac, E. Demler, M. D. Lukin, and P. Zoller, Majorana Fermions in Equilibrium and in Driven Cold-Atom Quantum Wires, *Phys. Rev. Lett.* **106**, 220402 (2011).
- [6] C. Chin and P. S. Julienne, Radio-frequency transitions on weakly bound ultracold molecules, *Phys. Rev. A* **71**, 012713 (2005).
- [7] G. Veeravalli, E. Kuhnle, P. Dyke, and C. J. Vale, Bragg Spectroscopy of a Strongly Interacting Fermi Gas, *Phys. Rev. Lett.* **101**, 250403 (2008).
- [8] S. Hoinka, P. Dyke, M. G. Lingham, J. J. Kinnunen, G. M. Bruun, and C. J. Vale, Goldstone mode and pair-breaking excitations in atomic Fermi superfluid, *Nat. Phys.* **13**, 943 (2017).
- [9] L. Pitaevskii and S. Stringari, *Bose-Einstein Condensation* (Oxford University Press, Oxford, 2003).
- [10] H. Hu, X.-C. Yao, and X.-J. Liu, Second sound with ultracold atoms: A brief historical account, *AAPPS Bull.* **32**, 26 (2022).
- [11] A. J. Leggett, Number-phase fluctuations in two-band superconductors, *Prog. Theor. Phys.* **36**, 901 (1966).
- [12] Y.-C. Zhang, S. Ding, and S. Zhang, Collective modes in a twoband superfluid of ultracold alkaline-earth-metal atoms close to an orbital Feshbach resonance, *Phys. Rev. A* **95**, 041603(R) (2017).
- [13] P. Zou, H. Zhao, L. He, X.-J. Liu, and H. Hu, Dynamic structure factors of a strongly interacting Fermi superfluid near an orbital Feshbach resonance across the phase transition from BCS to Sarma superfluid, *Phys. Rev. A* **103**, 053310 (2021).
- [14] D. Pekker and C. Varma, Amplitude/Higgs modes in condensed matter physics, *Annu. Rev. Condens. Matter Phys.* **6**, 269 (2015).
- [15] H. Zhao, X. Gao, W. Liang, P. Zou, and F. Yuan, Dynamical structure factors of a two-dimensional Fermi superfluid

- within random phase approximation, *New J. Phys.* **22**, 093012 (2020).
- [16] R. Combescot, S. Giorgini, and S. Stringari, Molecular signatures in the structure factor of an interacting Fermi gas, *Europhys. Lett.* **75**, 695 (2006).
- [17] A. Brunello, F. Dalfovo, L. Pitaevskii, S. Stringari, and F. Zambelli, Momentum transferred to a trapped Bose-Einstein condensate by stimulated light scattering, *Phys. Rev. A* **64**, 063614 (2001).
- [18] R. M. Lutchyn, J. D. Sau, and S. Das Sarma, Majorana Fermions and a Topological Phase Transition in Semiconductor-Superconductor Heterostructures, *Phys. Rev. Lett.* **105**, 077001 (2010).
- [19] X.-J. Liu and H. Hu, Topological superfluid in one-dimensional spin-orbit-coupled atomic Fermi gases, *Phys. Rev. A* **85**, 033622 (2012).
- [20] R. Wei and E. J. Mueller, Majorana fermions in one-dimensional spin-orbit-coupled Fermi gases, *Phys. Rev. A* **86**, 063604 (2012).
- [21] X.-J. Liu, Impurity probe of topological superfluids in one-dimensional spin-orbit-coupled atomic Fermi gases, *Phys. Rev. A* **87**, 013622 (2013).
- [22] Y. Xu, L. Mao, B. Wu, and C. Zhang, Dark Solitons with Majorana Fermions in Spin-Orbit-Coupled Fermi Gases, *Phys. Rev. Lett.* **113**, 130404 (2014).
- [23] X.-J. Liu, Soliton-induced Majorana fermions in a one-dimensional atomic topological superfluid, *Phys. Rev. A* **91**, 023610 (2015).
- [24] P. W. Anderson, Random-Phase Approximation in the Theory of Superconductivity, *Phys. Rev.* **112**, 1900 (1958).
- [25] A. Bulgac, Local-density-functional theory for superfluid fermionic systems: The unitary gas, *Phys. Rev. A* **76**, 040502(R) (2007).
- [26] P. Zou, E. D. Kuhnle, C. J. Vale, and H. Hu, Quantitative comparison between theoretical predictions and experimental results for Bragg spectroscopy of a strongly interacting Fermi superfluid, *Phys. Rev. A* **82**, 061605(R) (2010).
- [27] P. Zou, H. Hu, and X.-J. Liu, Low-momentum dynamic structure factor of a strongly interacting Fermi gas at finite temperature: The Goldstone phonon and its Landau damping, *Phys. Rev. A* **98**, 011602(R) (2018).
- [28] X.-J. Liu, H. Hu, A. Minguzzi, and M. P. Tosi, Collective oscillations of a confined Bose gas at finite temperature in the random-phase approximation, *Phys. Rev. A* **69**, 043605 (2004).
- [29] L. He and Z.-Q. Yu, Dynamic structure factors and sum rules in two-component quantum gases with spin-orbit coupling, *Acta Phys. Sin.* **65**, 131101 (2016).
- [30] G. Fan, X.-L. Chen, and P. Zou, Probing two Higgs oscillations in a one-dimensional Fermi superfluid with Raman-type spin-orbit coupling, *Front. Phys.* **17**, 52502 (2022).